www.rsya.org

Journal of Analytical Research

Vol 3 – Issue 1, Jan-Jun 2023

www.rsya.org/jar

Robotic Arc Welding Numerical Simulation for the Temperature Distribution

Annaranjan Rangaraju, Siva Kanti Prasad*

Sastra Deemed University, Trichy-Tanjore Road, Thirumalaisamudram, Thanjavur, Tamil Nadu 613401, India

*Corresponding Author: sivakanti230999@gmail.com

Abstract. The current investigation also used a numerical simulation run on a sample of an automated mild steel welded joint. The current numerical simulation includes a Gaussian-derived conical moving temperature source. Additionally, with a few small adjustments, the robot uses ANSYS to do thermally mechanical weld testing. Considering the mild steel's thermal and physical characteristics that affect the thermal conductivity of welding. We investigated how the parameters of the robotic arc welding process affected the shape of the weld bead and defined the analysis of temperature distribution using those factors. These variables included welding temperature, welding speed, and welding current. The distribution of temperature produced from numerical data is related to the experimental results. This form is an accurate approximation because it closely matches the outcomes of the weld zone profile's numerical simulation. Increased average power and slower welding speeds will result in higher peak temperature increases. For welding, the lowest temperature is 320 degrees Celsius at 27 millimetres per second and the highest temperature is 35 millimetres per second with an average power of 120 amps, according to measurements.

Keywords: ***Robotic Arc Welding, Numerical Simulation, Temperature Distribution, welded joint, ANSYS, welding current, welding speed, and welding temperature.***

1. Introduction

High-density welding can be done using robots because of their smoothness, accuracy, and efficiency. Numerical simulation has been created in this subject due to the complexity of robotic welding techniques and the necessity to better understand physical events occurring during the welding process. An automated method of welding, robotic welding, connects a wide variety of materials, both similar and different, without the need for human interaction. Robot welding has become a key area of study for a number of scholars during the past decade. The temperature profile and weld geometry were anticipated by the analysis and numerical simulation procedure for robotic arc welding. In response to new technologies and a growing need for development, the robotics

system began to change. An increasing number of manufacturers and researchers are looking at the design, control, and sensing capabilities of arc welding robots. The robot's ability to sense is another key component in the creation of an arc welding system. The parameters will be read by the centre welding sensor, and then an Optical Signal, Voltage, and Current will be interpreted from them. Welding always results in the formation of a localized coalescence, often known as a permanent joint, regardless of whether or not the filler material is put in conjunction with a separate filing joint. In most cases, the links are lined with the use of fasteners. On the basis of the heat source, Rosenthal has established an analysis method for the temperature distribution of welded joints. As long as the melting point is not exceeded by 30%, Rosenthal solutions are reliable. [1]. ANSYS APDL was used to create a three-dimensional heat flow model and investigate pulsed laser welding. [2-3] Laser welding 10mm thick 304L plates with a 15kW laser beam was tested for residual stresses. The laser welding temperature and tension were simulated using ABAQUS. Transient thermal analysis was used by [4] to mimic laser beam welding used FEA codes to compare experimental results for different laser welding process parameters, and the measurement of the temperature profile and weld geometry bead length and penetration depth) used finite element and finite differential weld temperature-geometric distribution methods to simulate laser pulse welding [5-6]. Laser spot welding heat flow with volumetric and surface heat flow was studied by [7]. The software from ANSYS was used to investigate TIG and laser-beam welding for INCONEL 625 and AISI316 [8]. AISI 316 and INCONEL 625 fusion zones were compared using TIG and laser welding. The 3-dimensional FEM model mimics the distribution of the temperature of the magnesium alloy and the shape of the laser weld beads [9–10]. Finite element code was utilised by [11–12] to simulate 304L pulsed-laser welding. To test the transient temperature distribution and welding perforation geometry of AISI 304L 1.6 mm thick laser welding T-joint sheet, a FEM code was developed. In order to create finite element patterns, the 2 mm thick, low carbon, mild stainless-steel residual stress and temporary temperature profile were analyzed in ANSYS. The temperature decreases quickly at first, then gradually as the thickness increases. Give an example of a finite element design that is equivalent (Ti6Al4V) and differential (AA5754 alloy and T40 layer pure titane) for predicting bead thermal appearance and form. Three-source laser beam welding is investigated [13-17]. Austenitic stainless steel 316L laser welding process factors are being examined in this study to see how they affect temperature distributions and welding geometry using an ANSYS APDL assembly. Thermal conductivity, specific heat, and density of the 1.4 mm thin 316L sheet were also examined. A three-dimensional conical Gaussian heat source is used in this simulation. In addition to the butt and T-joint welded constructions described above, large sophisticated Mag welded panel structures can be used in a wide variety of other sectors. [18-20] The ISM approach for welding panel deformations were developed. Thermal elastic polymers were used to simulate a small-scale model for ISM measurements (TEPs) [21- 24]. A more straightforward TEP method for residual-stress welding and deformation estimates was put forth by [25–26]. For the purpose of accelerating measurement, the required thermal boundary conditions have not been implemented to simulate electrode mobility with heat flow. In order to look for residues and strains in MAG butt-welded pipes, also analyzed welded MAG lap junctions [27-30].

2. Experimentation

2.1 Numerical Simulation

2.1.1 Temperature Distribution

The transient control equation for three-dimensional heat conduction is shown in the same way as in Eq. 1.

$$"\rho c\frac{\partial T}{\partial \tau}+v\rho c\frac{\partial T}{\partial y}=\frac{\partial}{\partial x}\ K_x\frac{\partial T}{\partial x}+\frac{\partial}{\partial y}(K_y\frac{\partial T}{\partial y}+\frac{\partial T}{\partial Z}\left(K_z\frac{\partial T}{\partial z}\right)+Q\ (x,y,z)" \qquad (1)$$

A conical heat source moving at v along the y axis is thought to have a Gaussian distribution that the welding temperature will follow. The robotic welding apparatus used in the current experiment is shown in Fig. 1, and robotic welding procedures are shown in Fig. 2. In an experiment, a mild steel workpiece absorbs 71.5 percent of the power while losing 40.2% of the total power. It is anticipated that it will absorb 16.8% of the power from the top surface temperature (Qsurf) of the welding workpiece and 48% from the material structure (Qkeyhole). Heat is distributed on the upper surface by Equation 2.

$$Q(x,y)=\frac{3Q_{surf}}{\pi R^2}e^{(-\frac{3(x^2+(y-v\times t)^2)}{R^2})} \qquad (2)$$

Qsurf derives its heat power from the plane's heat source (17.3 percent). For use in the keyhole simulation, Eq. 3 provides the Gaussian heat flux distribution.

$$Q(z)=\frac{2Q_{keyhole}}{\pi r_0^2 H}e^{1-(\frac{x^2+(y-v\times t)^2}{r_0})^2}(1-{}^{Z}/_{H}) \qquad (3)$$

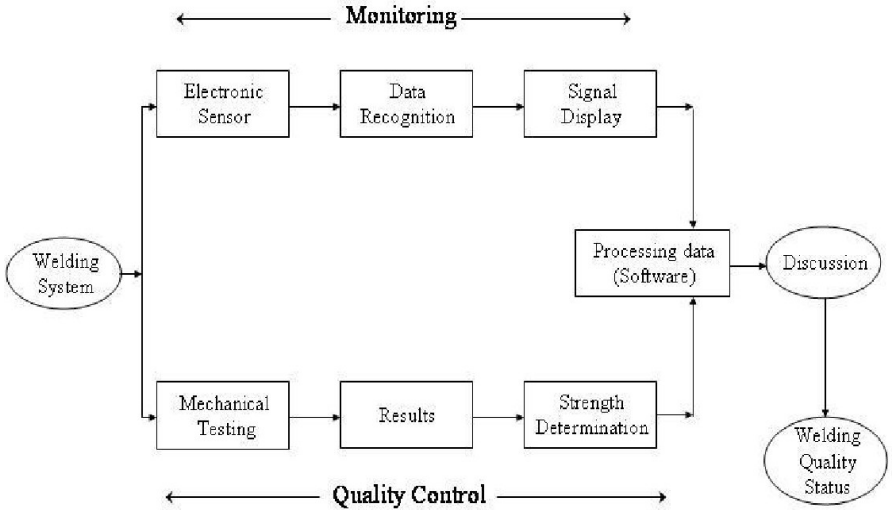

Figure. 1 arc robotic welding method representation [31]

3. METHODOLGY

The experimental equipment depicted in Figure 4 is a measurement system and data processing. An arc-welding robot was put through its paces during a trial run. Above the table, a bead of the same size was held. The V-Groove was filled to the top with a level surface. Welding with AWS A5.1 E 6013 was performed using ASTM A 36. Scale was 6 mm in length. 90A to 110A and 27 mm/sec welding current were used. Arduino (AT Mega 328p) was used to operate the sensors, which were then connected to a PC for processing and storing. Analyses of continuous data are carried out by the Arduino. A 110 A average current electrical arc weld was used to confirm the numerical temperature simulation results of a 6 mm thick mild steel. When the temperature range is between -40°C and 500°C, the thermostat is set at four distinct thermocouple K sites far enough away from

the weld lines to prevent damage to the welds, when using an 8mm weld bead, a medium beam force of 435°C, with a 27 mm/s welding speed.

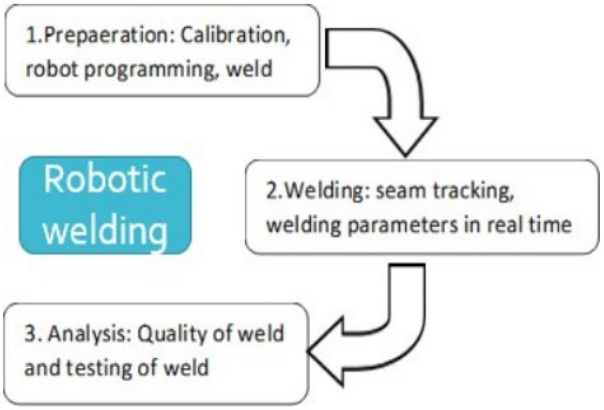

Figure. 2 Robotic welding processes [32]

The total amount of heat that surface and volume models have added to the model is seen in Eq. 4.

$$Q_v\,(r,z) = Q\,(x,y) + Q(z) \qquad (4)$$

4. Results and discussions

When different values for average welding current, welding velocity, and welding temperature are entered into ANSYS, the simulation results are as follows, mathematical computations are performed in order to determine the temperature distribution. The robotic welding settings described in Table 1 were used in a number of numerical simulations. Figure 5 illustrates the temperature transients that occur during robotic arc welding of mild steel when a constant welding speed of 27 mm/s and a welding bead diameter of 10 mm are used in conjunction with varying average temperatures ranging from 120 to 420 °C. Figure 4 depicts the influence that a peak temperature distribution has on the mean weld strength of a weld line. This effect was created by maintaining a constant welding speed of 27mm/s. Using a welding current ranging from 120-420 W and a velocity of 27 mm/s, figure 8 illustrates the three-dimensional distribution of thermal conductivity. Figure 7 is a visual representation of the influence that the welding current and the weld velocity have on the geometry of a weld bead that is 10 millimetres in diameter.

The average beam power as well as the welding speed both have an effect on the weld bead's geometric appearance. The shape of the weld beads resembled a H when they were subjected to high inputs (pressure speeds). The effects of temperature distribution were numerically obtained using thermocouples of the K type, which were placed in different spots. At a welding speed of V = 27 mm/s, steady-state thermal conditions, with both directed and total heat flux, and a temperature that fluctuates on average, Figure 8 shows the distribution of the three-dimensional temperature field. At a variety of locations (X) away from the weld line, a numerical simulation is compared to K-type thermo-pairs' temperature effects.

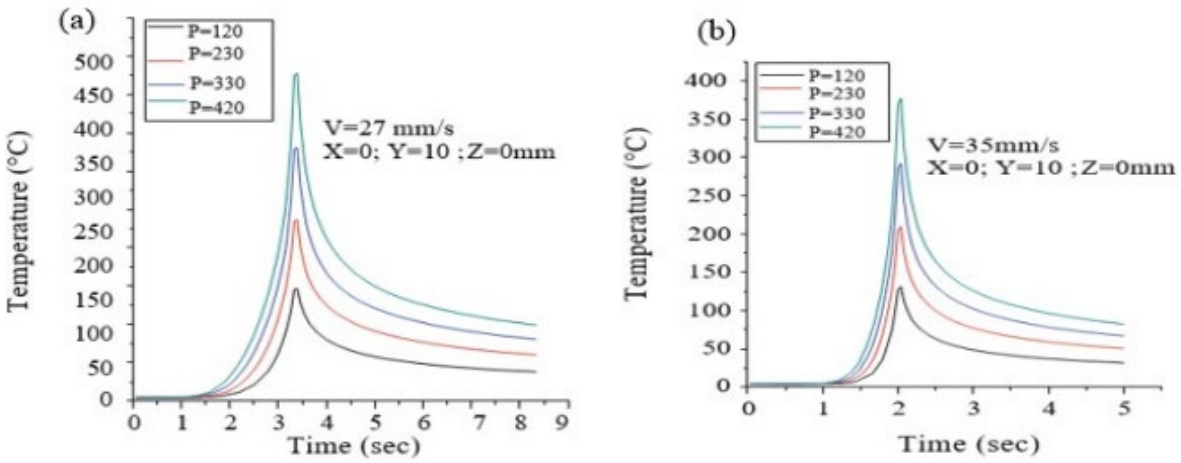

Figure. 5. Variable average temperatures in the temperature distribution between 27 and 35 mm/s along a continuous welding line

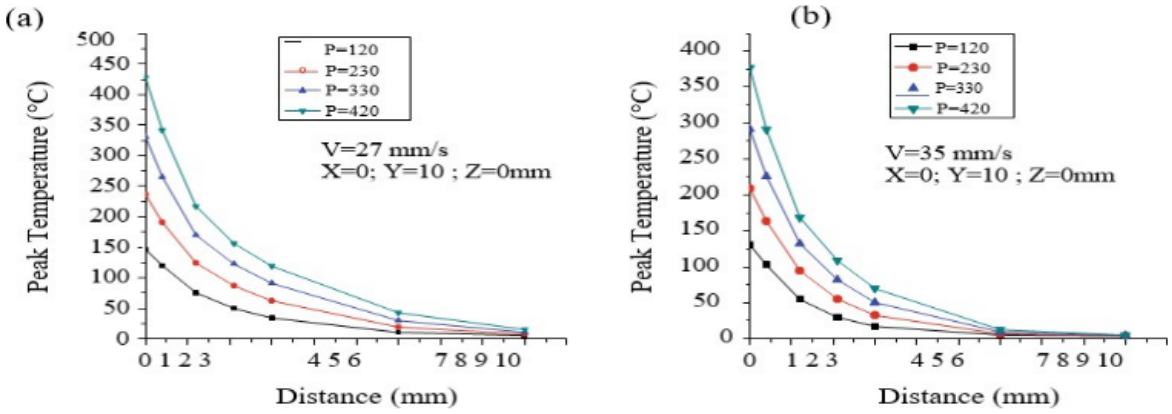

Figure 6. For consistent welding speeds outside from the weld line, use a peak-average temperature distribution.

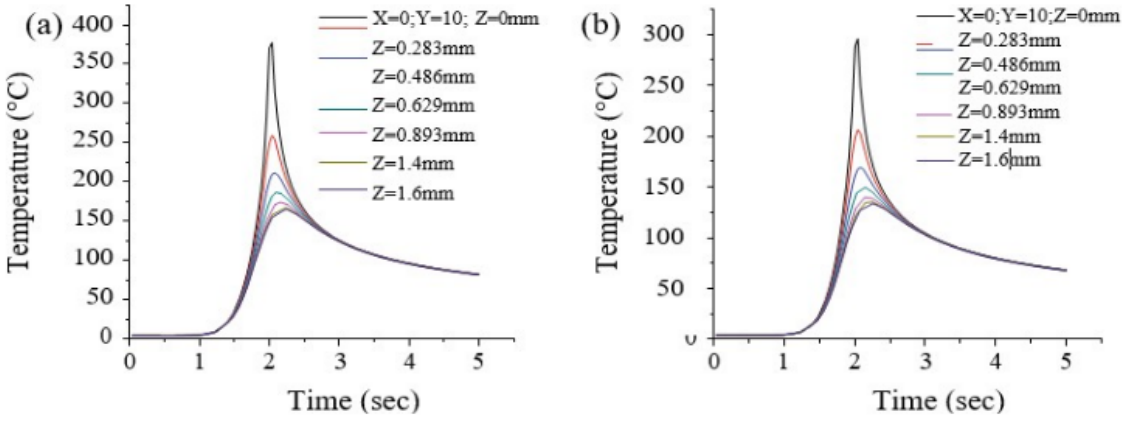

Figure 7. With a welding bead of 5 mm in diameter and a constant velocity of V = 27 mm/s, the maximum surface temperature change was 425 °C.

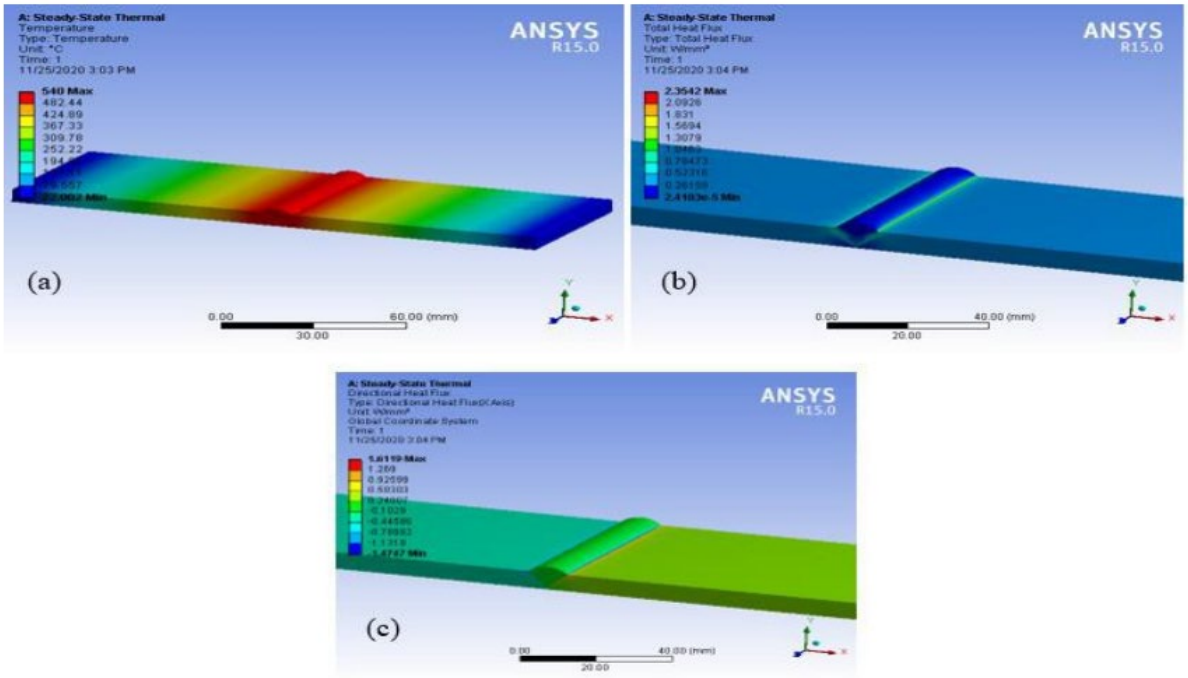

Figure. 8 (a), (b), (c) Steady-state temperature, total heat flux, directional heat flow with variable average temperature

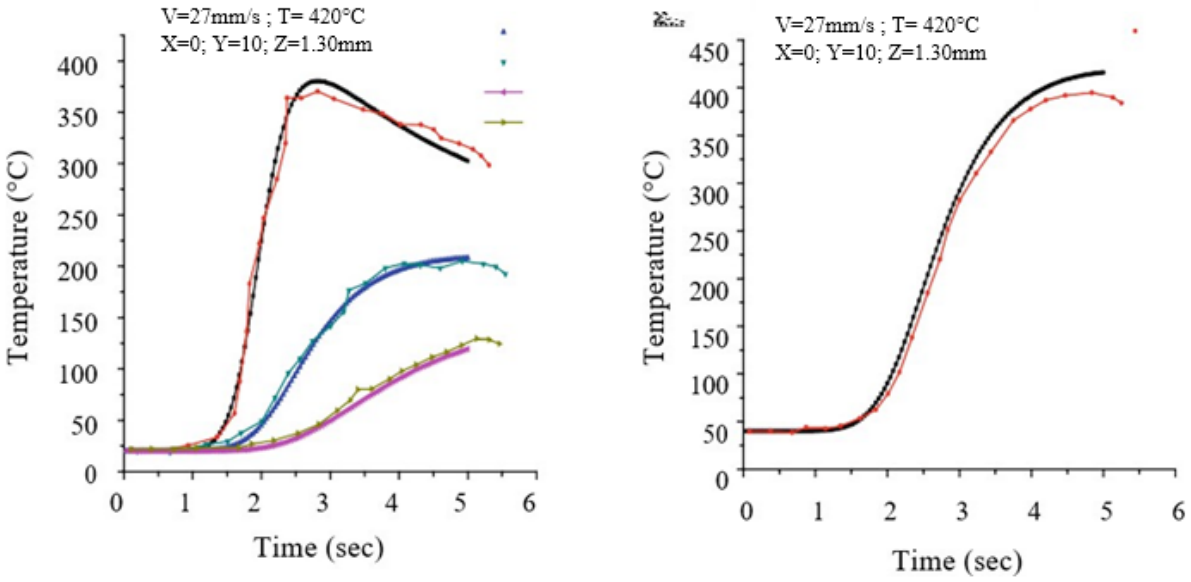

Figure 9. Modeling temperature effects (X) K-type thermo-pairs should be used away from the welding line.

5. Conclusion

Investigations were conducted into the characteristics of the robot arc welding process, including welding temperature, welding rate, and welding current, as well as their impact on temperature profiles, the shape and size of molten ponds, and bead geometries. The welding temperature, welding rate, and welding current are some of these characteristics. The numerical findings that were simulated were validated with the use of an experimental robotic welding value that had a satisfactory agreement. The following deductions are logically possible as a result of this investigation.

A rise in high temperatures will be observed if welding speed is maintained but average power is increased. The minimum temperatures for welding are measured to be 320 degrees Celsius at a welding speed of 27 millimetres per second with a typical welding current of 110 amps, while the highest temperatures for welding are measured to be 35 millimetres per second with an average power of 120 amps. The maximum temperature takes a considerable nosedive as soon as we go away from the weld line, where it was previously stable. When the temperature input is high enough, the geometry of the weld beads shifts into a shape that is almost identical to an H. The greatest temperature recorded by any one of the four K-type thermocouples was determined through the process of experiment.

References

[1] Rosenthal D(1946) The theory of moving sources of heat and its application of metal treatments. Trans ASME 68:849–866

[2] Frewin MR, Scott D (1999) Finite element model of pulsed laser welding. Weld J 78:15-s

[3] Carmignani C, Mares R, Toselli G (1999) Transient finite element analysis of deep penetration laser welding process in a single pass butt-welded thick steel plate. Comput Methods Appl Mech Eng 179(3):197–214

[4] Tsirkas SA, Papanikos P, Kermanidis T (2003) Numerical simulation of the laser welding process in butt-joint specimens. J Mater Process Technol 134(1):59–69

[5] Sabbaghzadeh J, AziziM, Torkamany MJ (2008) Numerical and experimental investigation of seam welding with a pulsed laser. Opt Laser Technol 40(2):289–296

[6] Balasubramanian KR, Siva Shanmugam N, Buvanashekaran G, Sankaranarayana-samy K (2008) Numerical and experimental investigation of laser beam welding of AISI 304 stainless steel sheet. Adv Prod Eng Manag 3(2):93–105

[7] Bag S, Trivedi A, De A (2009) Development of a finite element based heat transfer model for conduction mode laser spot welding process using an adaptive volumetric heat source. Int J Therm Sci 48(10):1923–1931

[8] Capriccioli A, Frosi P (2009) Multipurpose ANSYS FE procedure for welding processes simulation. Fusion Eng Des 84(2):546–553.

[9] A Kumar, K Sharma, AR Dixit A review of the mechanical and thermal properties of graphene and its hybrid polymer nanocomposites for structural applications, Journal of materials science 54 (8), 5992-6026.

[10] Belhadj A, Bessrour J, Masse JE, Bouhafs M, Barrallier L (2010) Finite element simulation of magnesium alloys laser beam welding. J Mater Process Technol 210(9):1131–1137.

[11] Kim K, Lee J, Cho H (2010) Analysis of pulsed Nd: YAG laser welding of AISI 304 steel. J Mech Sci Technol 24(11):2253–2259.

[12] A Kumar, K Sharma, AR Dixit A review of the mechanical and thermal properties of graphene and its hybrid polymer nanocomposites for structural applications, Journal of materials science 54 (8), 5992-6026.

[13] Shanmugam NS, Buvanashekaran G, Sankaranarayanasamy K, Kumar SR (2010) A transient finite element simulation of the temperature and bead profiles of T-joint laser welds.Mater Des 31(9):4528–4542

[14] Yilbas BS, Arif AFM, Aleem BA (2010) Laser welding of low carbon steel and thermal stress analysis. Opt Laser Technol 42(5):760–768

[15] K Sharma, M Shukla, Three-phase carbon fiber amine functionalized carbon nanotubes epoxy composite: processing, characterisation, and multiscale modeling, Journal of Nanomaterials 2014

[16] Casalino G, Mortello M, Contuzzi N, Minutolo FMC (2015) Finite element model for laser welding

of titanium. Procedia CIRP 33:434–439
[17] Chukkan JR, Vasudevan M, Muthukumaran S, Kumar RR, Chandrasekhar N (2015) Simulation of laser butt welding of AISI 316L stainless steel sheet using various heat sources and experimental validation. J Mater Process Technol 219:48–59.
[18] K Sharma, KS Kaushalyayan, M Shukla, Pull-out simulations of interfacial properties of amine functionalized multi-walled carbon nanotube epoxy composites, Computational Materials Science 99, 232-241.
[19] Deng, D.; Murakawa, H.; Liang, W. Prediction of Welding Distortion in a Curved Plate Structure by Means of Elastic Finite Element Method. J. Mater. Process. Technol. 2008, 203, 252–266.
[20] A Yadav, A Kumar, PK Singh, K Sharma, Glass transition temperature of functionalized graphene epoxy composites using molecular dynamics simulation, Integrated Ferroelectrics 186 (1), 106-114.
[21] Azad, N.; Iranmanesh, M.; Darvazi, A.R. A Study on the Effect of Welding Sequence on Welding Distortion in Ship Deck Structure. Ships Offshore Struct. 2019, 15, 355–367.
[22] PK Singh, K Sharma, A Kumar, M Shukla, Effects of functionalization on the mechanical properties of multiwalled carbon nanotubes: A molecular dynamics approach, Journal of Composite Materials 51 (5), 671- 680
[23] Zhang, Y.; Wang, Y. The Influence of Welding Mechanical Boundary Condition on the Residual Stress and Distortion of a Stiffened-Panel. Mar. Struct. 2019, 65, 259–270.
[24] Podder, D.; Gupta, O.P.; Das, S.; Mandal, N.R. Experimental and Numerical Investigation of Effect of Welding Sequence on Distortion of Stiffened Panels. Weld. World 2019, 63, 1275–1289.
[25] PK Singh, K Sharma, Mechanical and Viscoelastic Properties of In-situ Amine Functionalized Multiple Layer Grpahene/epoxy Nanocomposites, Current Nanoscience 14 (3), 252-262
[26] Peri´c, M.; Seleš, K.; Tonkovi´c, Z.; Lovreni´c-Jugovi´c, M. Numerical Simulation of Welding Distortions in Large Structures with a Simplified Engineering Approach. Open Phys. 2019, 17, 719–730.
[27] Wu, C.; Lee, C.; Kim, J.-W. Numerical Simulation of Bending Deformation Induced by Multi-Seam Welding of a Steel-Pipe Structure. J. Mech. Sci. Technol. 2020, 34, 2121–2131.
[28] Singh PK, & Sharma K, Molecular Dynamics Simulation of Glass Transition Behaviour of Polymer based Nanocomposites, Journal of Scientific & Industrial Research, 77 (10) (2018) 592-595
[29] Zhao, M.; Wei, F.; Huang, W.Q.; Lei, Y. Experimental and Numerical Investigation on Combined Girth Welding of API X80 Pipeline Steel. Sci. Technol. Weld. Join. 2015, 20, 622–630.
[30] Lin, J.; Ma, N.; Lei, Y.; Murakawa, H. Measurement of Residual Stress in Arc Welded Lap Joints by Cosα X-Ray Diffraction Method. J. Mater. Process. Technol. 2017, 243, 387–394.
[31] Anas Islam, Shailesh Sharma, Kamal Sharma, Rohit Sharma, Aman Sharma, Debanik Roy "Real-time data monitoring through sensors in robotized shielded metal arc welding" Materials today proceedings Volume 26, Part 2, 2020, Pages 2368-2373.
[32] Aman Sharma, Kamal Sharma, Anas Islam, Debanik Roy "Effect of welding parameters on automated robotic arc welding process" Materials today proceedings Volume 26, Part 2, 2020, Pages 2363-2367.